



Published in final edited form as:

*Nat Neurosci.* 2015 July ; 18(7): 988–996. doi:10.1038/nn.4024.

## The Human Epilepsy Mutation *GABRG2(Q390X)* Causes Chronic Subunit Accumulation and Neurodegeneration

Jing-Qiong Kang<sup>1</sup>, Wangzhen Shen<sup>1</sup>, Chengwen Zhou<sup>1</sup>, Dong Xu<sup>4</sup>, and Robert L. Macdonald<sup>1,2,3</sup>

<sup>1</sup>Department of Neurology, Vanderbilt University Medical Center; Nashville, TN

<sup>2</sup>Department of Molecular Physiology and Biophysics, Vanderbilt University Medical Center; Nashville, TN

<sup>3</sup>Department of Pharmacology, Vanderbilt University Medical Center; Nashville, TN

<sup>4</sup>Departments of Computer Science and Christopher S. Bond Life Sciences Center, University of Missouri, Columbia, MO

### Abstract

Genetic epilepsy and neurodegenerative diseases are two common neurological disorders conventionally viewed as being unrelated. A subset of patients with severe genetic epilepsies with impaired development and often death respond poorly to anticonvulsant drug therapy, suggesting a need for new therapeutic targets. Previously, we reported that multiple GABA<sub>A</sub> receptor epilepsy mutations caused protein misfolding and abnormal receptor trafficking. Here we establish in a novel model of a severe human genetic epileptic encephalopathy, the *Gabrg2*<sup>+/*Q390X*</sup> knock-in mouse, that in addition to impairing inhibitory neurotransmission, mutant GABA<sub>A</sub> receptor  $\gamma$ 2(Q390X) subunits accumulated and aggregated intracellularly, activated caspase 3 and caused widespread, age-dependent neurodegeneration. These novel findings suggest that the fundamental protein metabolism and cellular consequences of the epilepsy-associated mutant  $\gamma$ 2(Q390X) ion channel subunit are not fundamentally different from those associated with neurodegeneration. The study has far-reaching significance for identification of conserved pathological cascades and mechanism-based therapies that overlap genetic epilepsies and neurodegenerative diseases.

Users may view, print, copy, and download text and data-mine the content in such documents, for the purposes of academic research, subject always to the full Conditions of use:[http://www.nature.com/authors/editorial\\_policies/license.html#terms](http://www.nature.com/authors/editorial_policies/license.html#terms)

Corresponding Author: Jing-Qiong Kang, M.D., Ph.D., Vanderbilt University Medical Center, 6140 Medical Research Building III, 465 21st Ave, South, Nashville, TN 37232-8552, Tel: 615-936-8399; fax: 615-322-5517, [jingqiong.kang@vanderbilt.edu](mailto:jingqiong.kang@vanderbilt.edu).

**Author Contributions** J.Q.K. and R.L.M. conceived the project, and J.Q.K. designed experiments, performed experiments; analyzed the data; coordinated the study; supervised the project and wrote the manuscript. R.L.M. supervised the animal breeding to develop the congenic wild-type and mutant strains. W.S. collected the biochemical data and helped on colony maintenance, genotyping and tissue preparation. Z.C. collected and analyzed the electrophysiology data. X.D. performed the protein modeling and wrote the protein modeling part of the paper. R.L.M. supervised the project, critically reviewed the data and edited the manuscript. All authors discussed the results and commented on the manuscript.

Supplementary Information is available in the online version of the paper.

A Supplementary Methods Checklist is available.

## Keywords

GABA<sub>A</sub> receptors; genetic epilepsy;  $\gamma 2(Q390X)$  subunit mutation;  $\gamma 2(Q351X)$  subunit mutation; protein accumulation/aggregation; caspase 3 activation; neuronal death; *Gabrg2*<sup>+/*Q390X*</sup> knock-in mouse; SUDEP

## Introduction

Genetic epilepsies (GEs) are common neurological disorders that are associated frequently with ion channel gene mutations<sup>1</sup>. Although many GEs are relatively benign, there is a group of GEs, the epileptic encephalopathies including Dravet syndrome, which are associated with intractable seizures, impaired development, severe cognitive impairment and sudden death. It is not known, however, if the intractable seizures or some underlying progressive pathological processes are responsible for their clinical outcomes or if the clinical features of the epileptic encephalopathies are caused by the impaired channel function, the presence of intracellular mutant ion channel protein or both.

The epileptic encephalopathy, Dravet syndrome, has been shown to be associated with mutations in sodium channel (*SCN1A*, *SCN2A*, *SCN1B*)<sup>2-5</sup> and GABA<sub>A</sub> receptor (*GABRG2*<sup>6,7</sup>, *GABRA1*<sup>8</sup>) channel subunit genes. *GABRG2(Q390X)* is a mutation heterozygously associated with Dravet syndrome<sup>7</sup> (note: the *GABRG2(Q390X)* mutation is also referred to as *GABRG2(Q351X)*<sup>7,9,10</sup> when not including the 39 amino acid signal peptide). We have characterized extensively the cellular effects of this mutation *in vitro*<sup>9-11</sup> demonstrating that, like many other truncated proteins,  $\gamma 2(Q390X)$  subunits are nonfunctional. In addition, however, the subunits accumulated in the endoplasmic reticulum (ER) where they produced dominant negative suppression of the biogenesis and trafficking of wild-type subunits<sup>10</sup>. The  $\gamma 2(Q390X)$  subunits dimerized quickly once translated<sup>9</sup>, accumulated and disturbed cellular hemostasis in a concentration-dependent manner<sup>11</sup>. It is well established that sustained ER stress leads to neurodegeneration<sup>12</sup>; however, the long-term cellular consequences of a misfolded mutant ion channel subunit associated with GE have not been addressed.

Here we generated a heterozygous *Gabrg2*<sup>+/*Q390X*</sup> knock-in (KI) mouse and compared it to a heterozygous *Gabrg2*<sup>+/-</sup> knock-out (KO) mouse that has loss of functional  $\gamma 2$  subunits without accumulation of the mutant subunits. The *Gabrg2*<sup>+/-</sup> mouse has been reported to have mild hyperanxiety<sup>13</sup> and to have brief absence seizures only in mice with the seizure prone DBA2J genetic background<sup>14</sup>. In contrast, we found that *Gabrg2*<sup>+/*Q390X*</sup> mice had a severe epilepsy phenotype including spontaneous generalized tonic clonic seizures in mice with the seizure-resistant C57BL/6J background, suggesting that the mutation produced epilepsy by a mechanism(s) other than simple haploinsufficiency. Furthermore, we demonstrated that *Gabrg2*<sup>+/*Q390X*</sup> mice had increased mortality, reminiscent of sudden unexpected death in epilepsy (SUDEP) in humans. We compared the KI and KO mice functionally and biochemically and found that *Gabrg2*<sup>+/*Q390X*</sup> mice formed intraneuronal detergent-resistant, high molecular mass protein complexes containing  $\gamma 2$  subunits and displayed widespread caspase 3 activation and sporadic neuronal death in the mouse brain, especially in the cortex, that increased in severity with aging. This thus provides evidence

that an epilepsy ion channel gene mutation directly causes chronic neurodegeneration *in vivo*, and the presence of neurodegeneration in addition to intractable seizures provides a possible explanation, at least in part, for several key features of epileptic encephalopathies including the bases for phenotypic severity, drug resistance, progressive course and poor outcome. The findings suggest that the protein metabolism of an ion channel epilepsy mutation is not fundamentally different from that associated with neurodegeneration, and thus drugs developed to treat neurodegeneration might be repurposed to treat severe genetic epilepsies by targeting the same mechanisms.

## Results

### Mutant $\gamma 2(Q390X)$ subunits are aggregation-prone

GABA<sub>A</sub> receptors are the major mediators of inhibitory neurotransmission in the brain and are primarily composed of 2 $\alpha$ , 2 $\beta$  and 1 $\gamma$  subunits (Supplementary Fig. 1a). The *GABRG2(Q390X)* mutation was identified in two separate pedigrees with epilepsy including Dravet syndrome<sup>7</sup> and produces a truncated subunit with loss of 78 C-terminal amino acids (Supplementary Fig. 1b). We used protein structure modeling of the wild-type and mutant  $\gamma 2$  subunits without the extracellular N-terminal domain to predict the potential consequences on structure of the mutant subunit. For the mutant  $\gamma 2(Q390X)$  subunit, the hydrophobic 4<sup>th</sup> transmembrane  $\alpha$ -helix (YARIFFPTAFCLFNLVYWVSYLYL) was deleted, and a new  $\alpha$ -helix with many charged amino acids (KDKDKKKKNPAPTIDIRPRSATI) was found to assume its location (Fig. 1a). The upper domain of the wild-type  $\gamma 2$  subunit is mainly hydrophobic (Fig. 1a, left panel green) and embedded in the membrane as a transmembrane domain, while the lower domain is hydrophilic and intracellular (Fig. 1a, left panel red). The mutant  $\gamma 2(Q390X)$  subunit has more hydrophilic surface area than the wild-type subunit (Fig. 1b, left and middle panel) due to the new  $\alpha$ -helix (KDKDKKKKNPAPTIDIRPRSATI) that was found to be unstable in the membrane, thus changing the subunit from a transmembrane protein to a globular cytosolic protein. The remaining hydrophobic surfaces in the  $\alpha$ -helices of the mutant subunit were no longer in the membrane and were predicted to become “sticky” in solvent, i.e. the domains were predicted to bind to each other or to other proteins due to hydrophobic interactions. Based on a docking study for multiple interacting molecules, a number of relatively stable homo-dimer conformations may be formed as a result of non-specific self-interactions of mutant  $\gamma 2$  subunits (Supplementary Fig. 1c), and a number of non-specific hetero-dimer conformations may be formed between the mutant  $\gamma 2$  subunit and its wild-type partnering  $\alpha 1$  subunit (Supplementary Fig. 1d). All of these subunit dimers were predicted to be stable.

### The *GABRG2(Q390X)* mutation promoted intraneuronal accumulation of mutant $\gamma 2(Q390X)$ subunits in *Gabrg2<sup>+Q390X</sup>* KI mice

To fully characterize the pathological basis for the epilepsy associated with the Q390X mutation, we generated the heterozygous *Gabrg2<sup>+Q390X</sup>* KI mouse line with a standard gene targeting strategy (Fig. 1b). In both transfected HEK 293T cells and in brains from 1 week to 14 month old *Gabrg2<sup>+Q390X</sup>* mice, mutant  $\gamma 2(Q390X)$  subunits formed oligomers, likely dimers, tetramers and/or high molecular mass protein complexes on SDS-PAGE (Fig. 1c, blue arrows). The predicted molecular mass of the mutant  $\gamma 2(Q390X)$  subunit was 40

KDa, (Fig. 1c, red arrows), and the full length wild-type  $\gamma 2$  subunit was about 50 KDa<sup>10</sup> (Fig. 1c, green arrows). In HEK 293T and COS-7 cells cotransfected with  $\alpha 1$ ,  $\beta 2$  and  $\gamma 2(Q390X)^{YFP}$  subunits and in cultured rat cortical neurons transfected with  $\gamma 2^{YFP}$  or  $\gamma 2^{YFP}$  and  $\gamma 2(Q390X)^{YFP}$  subunits alone, the mutant subunits accumulated intracellularly in the ER (Fig. 1d).

Immunohistochemical staining with anti  $\gamma 2$  subunit antibody indicated consistently that  $\gamma 2$  subunits accumulated in the cortex of 2 and 16 month old KI mice (Fig. 1e–g) as well as in P0 KI mice and in multiple brain regions including the cortex (Supplementary Fig 2.). The  $\gamma 2$  subunit fluorescence intensity was increased in cultured neurons ( $22.20 \pm 0.97$  vs  $37.20 \pm 2.5$ ,  $n = 5$  cultures,  $p = 0.0005$ , unpaired t test) as well as in *Gabrg2<sup>+/Q390X</sup>* mice at both 2–4 and 16 months old (Fig. 2h). In the brains of P0 mice, the  $\gamma 2$  subunit staining was also stronger in *Gabrg2<sup>+/Q390X</sup>* than in wild-type mice, and in cerebellum  $\gamma 2$  subunit staining was prominent in the Purkinje cells layer, which contains Purkinje cells and Bergmann glia cells (Supplementary Fig. 2). The increased  $\gamma 2$  subunits in the somatic regions in *Gabrg2<sup>+/Q390X</sup>* mice across different ages suggest that there was consistent ER retention of the mutant subunit protein.

### ***Gabrg2<sup>+/Q390X</sup>* KI mice had reduced viability**

SUDEP is a significant concern for patients with epilepsy, especially those with frequent and severe seizures such as those associated with Dravet syndrome<sup>15</sup>. SUDEP has been characterized in the SCN1A KO mouse model of Dravet syndrome<sup>16</sup>, but the basis for SUDEP is still unclear. SUDEP could be due to brain driven cardiac dysfunction during seizures or to other non-cardiac mechanisms<sup>15, 17</sup>. Because the *GABRG2(Q390X)* mutation is associated with Dravet syndrome, we determined the mortality rate of heterozygous KI mice. We genotyped all mice by PCR of tail DNA (Fig. 2a), and included all of the retrieved dead pups. We found that heterozygous and homozygous KI mice were born with a reduced Mendelian ratio (Fig. 2b). Homozygous *Gabrg2<sup>Q390X/Q390X</sup>* mice, however, did not survive beyond the day of birth (Fig. 2e, asterisk), consistent with a previous report for homozygous *Gabrg2<sup>+/-</sup> KO mice*<sup>18</sup>. However, gross morphology of heterozygous and homozygous mice (Fig. 2c), and the cellular structure of heterozygous pup's brains (Fig. 2d) appeared to be normal. Although viable, heterozygous mice had increased mortality throughout life (measured up to 30 weeks), and wild-type mice had minimal to no death over that time period (Fig. 2e). The increased death rate for heterozygous KI mice was likely related to severe generalized seizures consistent with our observation that several mice died after the occurrence of spontaneous generalized tonic clonic seizures during routine handling.

### ***Gabrg2<sup>+/Q390X</sup>* KI mice had spontaneous seizures and neurobehavioral comorbidities**

We observed spontaneous generalized tonic clonic seizures in *Gabrg2<sup>+/Q390X</sup>* mice at 19 days old (Supplementary Fig. video showing a 19 day old heterozygous KI mouse with spontaneous generalized tonic clonic seizures and death). To characterize the seizure phenotype of heterozygous KI mice, we recorded synchronized video EEGs in mice. The EEGs demonstrated occurrence of spontaneous electrographic and behavioral seizures as well as interictal discharges (Fig. 3a, Supplementary Fig. 3). With blockade of GABA<sub>A</sub> receptors by pentylenetetrazol (PTZ; 50 mg/kg), heterozygous KI mice had lowered seizure

threshold compared with wild-type littermates as demonstrated by early onset and increased percentage of clonic seizures and tonic hind limb extension (Fig. 3b, c). The reason we chose a lower dose of PTZ was due to the high mortality rate of *Gabrg2<sup>+/-Q390X</sup>* mice at higher doses of PTZ (70 mg/kg or 85 mg/kg).

We then assessed potential behavioral comorbidities of epilepsy in *Gabrg2<sup>+/-Q390X</sup>* mice. We performed the elevated zero maze (EZM) test and the open field (OF) test. In the EZM test, heterozygous mice spent significantly less time in the open arm ( $121.6 \pm 6.46$  vs  $94.5 \pm 3.67$ ,  $n = 59$  for wt and  $57$  for het, unpaired t test) and had reduced total entries into the open arm ( $16.24 \pm 0.91$  vs  $13.39 \pm 0.61$ ,  $n = 59$  for wt and  $57$  for het, unpaired t test). In the OF test, heterozygous KI mice had increased total distance travelled in the first 10 minutes ( $1245.4 \pm 31.2$  vs  $1497.4 \pm 54.1$ ,  $n = 35$  for wt and  $47$  for het, unpaired t test) but tended to be quiet and stayed in the corner of the chamber in the later time segments and had reduced time spent in the center ( $31.28 \pm 1.113$  vs  $19.77 \pm 1.010$ ,  $n = 35$  for wt and  $47$  for het,  $p < 0.0001$ , unpaired t test). We could not exclude the possibility that the heterozygous KI mice had behavioral arrest after they were habituated in the testing chamber during the later time segments of the one hour long test. This was consistent with the fact that the KI mice spent less time in the center resting ( $42.98 \pm 2.58$  (sec) vs  $33.72 \pm 2.42$  (sec),  $n = 35$  for wt and  $47$  for het,  $p = 0.012$ , unpaired t test) and more time in the periphery resting ( $81.06 \pm 6.33$  vs  $106.4 \pm 5.82$ ,  $n = 35$  for wt and  $47$  for het,  $p = 0.045$ , unpaired t test). *Gabrg2<sup>+/-Q390X</sup>* mice had multiple phenotypes including spontaneous seizures, SUDEP, enhanced anxiety and deficits in social behaviors while *Gabrg2<sup>+/-</sup> KO mice* were reported to be seizure free<sup>13</sup> or to only have absence epilepsy in a specific seizure prone genetic background<sup>14</sup>.

### **GABAergic mIPSC amplitude and frequency were reduced more in *Gabrg2<sup>+/-Q390X</sup>* KI mice than in *Gabrg2<sup>+/-</sup> KO mice***

*Gabrg2<sup>+/-Q390X</sup>* KI mice had severe epilepsy, increased mortality and neuropsychiatric comorbidities. By contrast, *Gabrg2<sup>+/-</sup> KO mice* were reported to be seizure free<sup>13</sup> or to only have absence epilepsy, but not thermal seizures, in a specific seizure prone genetic background like DBA2J<sup>14</sup>. We next sought to determine if there was a difference in GABAergic synaptic strength between these animals. It is generally believed that a loss of function mutation such as a truncation mutation causes disease because of haploinsufficiency of the affected gene, and thus KO models have been widely used for studying human diseases<sup>19</sup>. We previously demonstrated *in vitro* that in addition to being nonfunctional, mutant  $\gamma 2(Q390X)$  subunits suppressed the biogenesis and function of wild-type partnering subunits<sup>9</sup>. To determine the impact of mutant  $\gamma 2(Q390X)$  subunits on GABAergic neurotransmission in KI mice, we recorded GABAergic mIPSCs in cortical layer VI neurons in age-matched *Gabrg2<sup>+/-Q390X</sup>* and *Gabrg2<sup>+/-</sup> KO mice*<sup>20</sup>. The choice of cortical layer VI neurons was based on the involvement of thalamocortical circuitry in seizure generation and neurons in this layer as well as the layer IV receive direct projection of ventrobasal complex (VB) neurons<sup>21</sup>. Compared with wild-type mice, heterozygous KI mice had reduced mIPSC amplitudes (Fig. 4a, c) and frequency ( $2.94 \pm 0.34$  vs  $1.69 \pm 0.40$ ,  $n = 16$  cells from 11 slices from 7 mice for wt,  $n = 13$  cells from 8 slices from 6 mice for het, unpaired t test,  $p = 0.021$ ), while there was no significant difference between wild-type and heterozygous KO mice in either amplitude (Fig. 4b, d) or frequency ( $3.61 \pm 0.91$  vs  $2.58 \pm$

0.29,  $n = 8$  cells from 6 slices from 5 mice for wt,  $n = 9$  cells from 7 slices from 6 mice for het, unpaired t test,  $p = 0.28$ ).

### **Although both *Gabrg2*<sup>+/<sup>Q390X</sup></sup> KI and *Gabrg2*<sup>+/-</sup> KO mice both had loss of $\gamma 2$ subunit function, biogenesis of the remaining wild-type partnering subunit differed between KI and KO mice**

The reduced mIPSC amplitude and frequency in *Gabrg2*<sup>+/<sup>Q390X</sup></sup> mice were likely due in part to the reduction of wild-type  $\gamma 2$  subunits but also secondarily to loss of  $\alpha 1$  subunits as a consequence of reduced  $\alpha 1\beta\gamma 2$  receptors being assembled and trafficked to synapses. This is not surprising given the critical role of  $\gamma 2$  subunits in synaptic GABA<sub>A</sub> receptor maintenance and clustering<sup>22</sup>. Consistent with the electrophysiological recordings, biochemical studies demonstrated that total levels of both wild-type  $\gamma 2$  and  $\alpha 1$  subunits were reduced in multiple brain regions including cortex in the KI mice (Fig. 5a, c, e, g and Supplementary Fig. 4 for full-length gels), while total levels of  $\gamma 2$  were reduced to a lesser extent and total levels of  $\alpha 1$  subunits were unaltered in the age matched heterozygous KO mice (Fig. 5b, d, f, h and Supplementary Fig. 4 for full-length gels). Such results suggest more impaired neuronal inhibition in the KI than in the KO mice. The data also suggested that the mutant  $\gamma 2(Q390X)$  subunits suppressed the biogenesis of their wild-type partnering subunits and wild-type  $\gamma 2$  subunits.

### **Younger *Gabrg2*<sup>+/<sup>Q390X</sup></sup> KI mice had intraneuronal accumulation of $\gamma 2$ subunits and reduced $\gamma 2$ subunits at synaptosomes and the cell surface in cerebral cortex**

Our *in vitro* study indicated that mutant  $\gamma 2(Q390X)$  subunits failed to traffic to the cell surface<sup>10</sup> and accumulated inside neurons. Here we demonstrated in *Gabrg2*<sup>+/<sup>Q390X</sup></sup> mice that the staining of  $\gamma 2$  subunits was more intense in neuronal somata compared with the age and gender matched wild-type littermates at 6 months old (Fig. 6a–c). However, the fluorescence signal intensity in the whole field or non-somatic regions was reduced in the *Gabrg2*<sup>+/<sup>Q390X</sup></sup> mice (Fig. 6a–c). The  $\gamma 2$  subunit puncta were colocalized with the inhibitory postsynaptic marker gephyrin. We further compared the distribution of the  $\gamma 2$  subunits in wild-type and heterozygous KI mice in synaptosomes or at the cell surface by subcellular fractionation or live brain slice surface biotinylation. The data demonstrated that the  $\gamma 2$  subunits were reduced in the synaptosomes (Fig. 6d, f and Supplementary Fig. 4 for the full-length gel) and at the cell surface (Fig. 6e, g and Supplementary Fig. 4 for the full-length gel). In summary, the data suggested that  $\gamma 2$  subunits in the synapses were reduced in spite of their accumulation in the neuronal somatic region.

### **Older mutant *Gabrg2*<sup>+/<sup>Q390X</sup></sup> KI mice had increased caspase 3 activation and cell death in the cerebral cortex**

Although no *in vivo* evidence for neurodegeneration in genetic epilepsy has been reported previously, in multiple neurodegenerative diseases it has been established that sustained accumulation and aggregation of mutant protein will lead eventually to neurodegeneration<sup>23–26</sup>. Thus, since the mutant  $\gamma 2(Q390X)$  subunit was aggregation prone and relatively stable<sup>9</sup>, its sustained expression could lead to neurodegeneration. To determine neuronal apoptosis in heterozygous KI mice, we stained for  $\gamma 2$  subunits and cleaved caspase

3 in 1 year old mice (Fig. 7a, b). Cleaved caspase 3 has been used as a marker for cellular apoptosis because of its role in executing cell death<sup>27</sup>. In *Gabrg2*<sup>+/*Q390X*</sup> KI, but not wild-type, mice, increased cleaved caspase 3 staining and  $\gamma 2$  subunit accumulation were both present in the deep layers of the cortex (Fig. 7a, b). The intensity of both  $\gamma 2$  subunit and cleaved caspase 3 staining was higher in the neuronal somata of the mutant than in wild-type mice (Fig. 7f). Cleaved caspase 3 was mainly in the neuronal cytoplasm (Fig. 7c) and colocalized with  $\gamma 2$  subunits in what appeared to be aggregates (Fig. 7d). These cleaved caspase 3/ $\gamma 2$  subunit aggregates were absent in the old wild-type and young (2 month) KI mice. They were detectable in the 5–6 month old KI mice but were prominent in old (1 year or older) KI mice with neuronal loss in the cortex (Supplementary Fig. 5–8). Paraffin-embedded brain tissues were used here because the staining was focused on neuronal somatic regions. Synaptic proteins were poorly preserved in these tissues compared with those with short fixation (Figs. 1f–g, 6a–b and Supplementary Fig. 9).

We also determined if the mutant  $\gamma 2$  subunit aggregates were associated with neuronal death. To do this, we performed TUNEL staining, and the percent of neurons with TUNEL positive staining in cortical layer V–VI neurons was higher in 1 year old heterozygous mice (Fig. 7e, g). It is believed that age is a risk factor for neurodegeneration and protein aggregation, and this concept has been well studied in neurodegenerative diseases caused by both genetic and environmental factors<sup>28–31</sup>. Our data are consistent with the studies of neurodegeneration; the older heterozygous mice had cleaved caspase 3 activation, cytoplasmic caspase 3/ $\gamma 2$  subunit positive aggregates and neuronal death while these features were not prominent in the younger *Gabrg2*<sup>+/*Q390X*</sup> mice (Supplementary Fig. 5–8, 10–12).

### **The activation of caspase 3 could be due to the accumulation of mutant $\gamma 2$ (Q390X) subunits independent of seizure activity**

Although caspase 3 activation is a crucial event for neuronal death and an established feature of many neurodegenerative diseases<sup>32</sup>, caspase 3 activation can be caused by other neuronal activities<sup>33</sup>. We thus determined the level of caspase 3 activation in cultured neurons where no seizure activity was present. We demonstrated that more neurons were positively stained with caspase 3 in the neurons cultured from the heterozygous *Gabrg2*<sup>+/*Q390X*</sup> mice than from the wild-type mice ( $4.6 \pm 1.7\%$  vs  $29.4 \pm 6.7\%$ ,  $n = 4$  cultures,  $p = 0.015$ , unpaired t test, Fig. 8a). In HEK 293T cells, we expressed wild-type  $\gamma 2$  or mutant  $\gamma 2$ (Q390X) subunits with progressively increased cDNA amounts and found that the mutant  $\gamma 2$ (Q390X) subunits had increased ER stress as evidenced by the upregulated expression of ER stress hallmark GADD153 (Fig. 8b, c). Interestingly, the wild-type  $\gamma 2$  subunits also increased ER stress with high amounts of transfected cDNA. This suggests that wild-type  $\gamma 2$  subunits also caused ER stress when assembly partners are lost and when they are present at high intracellular levels. The sustained ER stress would lead to cell death as evidenced by increased caspase 3 activation in the cells expressing the mutant  $\gamma 2$ (Q390X) subunit. The expression level of caspase 3 in the cells expressing mutant  $\gamma 2$ (Q390X) subunits was similar to the control cells treated with the apoptosis-inducer staurosporine (3  $\mu$ M) for 4 hrs (Fig. 8d); in contrast, caspase 3 activation was not or only minimally present

in the cells expressing wild-type  $\gamma 2$  subunits (Fig. 8e and Supplementary Fig. 4 for the full-length gel).

## Discussion

Dravet syndrome is an epileptic encephalopathy in which “the epileptic activity itself may contribute to severe cognitive and behavioral impairments above and beyond what might be expected from the underlying pathology alone (e.g., cortical malformation), and that these can worsen over time”<sup>34</sup>. However, the present work suggests that in addition to the disinhibition produced by substantial loss of functional  $\gamma 2$  subunits leading to epilepsy, the progressive behavioral changes and worsening epilepsy caused by the *GABRG2(Q390X)* mutation may also be due to neuronal dysfunction/neurodegeneration caused by the accumulation and aggregation of a truncated ion channel protein that increases cell stress and leads to chronic neurodegeneration.

There are no reports that the mutant protein associated with Dravet syndrome causes neurodegeneration. However, while not definitive, there are however several lines of evidence that neurodegeneration may occur in a subset of patients with GE. For example, a recent study of a brain specimen from a Dravet syndrome patient harboring the *GABRG2(Q40X)* mutation indicated that the mutant  $\gamma 2$  subunits formed protein aggregates, but the details of the aggregates are not available<sup>6</sup>. Our *in vitro* study indicated that mutant  $\gamma 2(Q390X)$  subunits produced substantial protein aggregates while mutant  $\gamma 2(Q40X)$  subunits were undetectable (Supplementary Fig. 13). In addition, a study using brain MRI in a large group of GE patients<sup>35</sup> found significant cortical atrophy, suggesting possible neuronal loss. A brain morphometry study in Dravet syndrome patients indicated global volume reductions of gray and white matter as well as a correlation between the intracranial volume reduction and increased age<sup>36</sup>. The lack of clear clinical evidence of an association of mutations in GE and neurodegeneration may be because epileptic encephalopathies occur in only a small subset of epilepsy patients and thus the relationship may possibly have been unrecognized. Also, the major cause of Dravet syndrome is *SCN1A* mutations, which may have a different pathophysiology than *GABRG2* mutations.

In Dravet syndrome, altered neurotransmission and seizure phenotypes have been extensively characterized in an *Scn1a* KO mouse as well as in a nonsense mutation *Scn1a* KI mouse<sup>37, 38</sup>. However, no mutant protein was detected in *Scn1a* KI mice, suggesting haploinsufficiency. In the present study, we showed that truncated  $\gamma 2(Q390X)$  subunits were produced, that they accumulated in neurons and that in older *Gabrg2<sup>+/Q390X</sup>* KI mice they formed sporadic protein aggregates in multiple brain regions. These findings are consistent with the wide spread expression of  $\gamma 2$  subunits in the brain<sup>39</sup>. We previously reported that mutant  $\gamma 2(Q390X)$  subunits produced dominant negative suppression of wild-type partnering and wild-type  $\gamma 2$  subunits<sup>10</sup>, and had slow degradation and disturbed cellular homeostasis<sup>26</sup>. The current study provides the novel findings that an ion channel mutation associated with a severe GE results in activated caspase 3, protein aggregates and chronic neurodegeneration.



*Gabrg2*<sup>+/*Q390X*</sup> KI mice phenocopy the major symptoms of the human epileptic encephalopathy, Dravet syndrome, and the phenotypes of patients that heterozygously carry the mutation (See patient natural history in Online Methods for full details.).

*Gabrg2*<sup>+/*Q390X*</sup> KI mice had multiple forms of epilepsy, including generalized tonic clonic seizures, neuropsychiatric comorbidities, including increased anxiety and social deficits and SUDEP. However, we did not find a difference in motor coordination between control and mutant mice up to age 6 months as demonstrated by the rotarod test. This is in contrast to the findings that there was severe ataxia in heterozygous *Scn1a*<sup>+/-</sup> KO mice at P21<sup>40</sup>. This suggests that there may be differences in the comorbidities between the severe epilepsies associated with an *SCN1A* mutation and a *GABRG2* mutation.

Comparison of *Gabrg2*<sup>+/*Q390X*</sup> KI and *Gabrg2*<sup>+/-</sup> KO mice demonstrated that GABAergic neurotransmission in KI mice was not equivalent to the simple loss of one allele in KO mice. The difference in GABAergic neurotransmission between the KI and KO mice was likely due to differences in wild-type GABA<sub>A</sub> receptor subunit biogenesis. *Gabrg2*<sup>+/-</sup> KO mice only had a small reduction of  $\gamma$ 2 subunits while  $\alpha$ 1 subunit expression was unchanged. In contrast, total expression of both  $\alpha$ 1 subunits and the remaining wild-type  $\gamma$ 2 subunits in *Gabrg2*<sup>+/*Q390X*</sup> mice was reduced in all the major brain regions including cerebral cortex, cerebellum, hippocampus and thalamus compared to wild-type littermates and to the *Gabrg2*<sup>+/-</sup> KO mice. This dominant negative suppression of the wild-type subunits by  $\gamma$ 2(Q390X) subunits is likely due to oligomerization of mutant  $\gamma$ 2(Q390X) subunits with wild-type subunits, thus trapping the wild-type subunits in the ER. This likely explains in part why *Gabrg2*<sup>+/*Q390X*</sup> KI mice had a more severe epilepsy phenotype.

This study challenges the widely held belief that neurodegeneration does not occur in GEs. Much effort has been directed to identify neuronal death in different animal models of epilepsy eg, pilocarpine, kainic acid kindling and thermal animal models<sup>41</sup>. However, these are models of acquired, not genetic, epilepsies. The cellular environment in *Gabrg2*<sup>+/*Q390X*</sup> mice is different than in the external stimulus-induced seizure models because the mutation is present from conception. We demonstrated that the KI mice had intraneuronal  $\gamma$ 2 subunit/caspase 3 protein aggregates and had caspase 3 activation and chronic neurodegeneration, although these features were not present in younger mice expressing the mutant subunit. The reduction of neuronal number was 15% in the somatosensory cortex in the old KI mice as marked by neuronal marker NeuN. However, sporadic neuronal death was observed in multiple brain regions including cortex, hippocampus, thalamus and cerebellum. In a given neuron, its viability and caspase 3 activation were likely correlated with the abundance of  $\gamma$ 2(Q390X) subunits. We have previously demonstrated that ER-retained trafficking-deficient  $\gamma$ 2 subunits produce ER stress<sup>11</sup>. It is possible that the activated caspase 3 also alters synaptic activity since caspase 3 is required for the refinement of neuronal circuits during development that involves selective elimination of axons, dendrites and synaptic connections<sup>32, 33</sup>. However, it should be noted that while mutant  $\gamma$ 2 subunits accumulated in neurons of mice at all ages, the neuronal death in the KI mice was highly variable, chronic and subject to substantial developmental impact being only evident in the older mice. The identification of mutant protein aggregation in *Gabrg2*<sup>+/*Q390X*</sup> KI mice has far reaching implications for both disease classifications and therapeutic strategies. Although GE and

neurodegenerative diseases are two conventionally unrelated disease entities, this study suggests that the mutant protein metabolism and the engaged signaling pathways like caspase 3 activation may be similar in both disorders. Therefore the therapeutic developments in neurodegeneration and other diseases with similar mechanisms could be repurposed to treat epilepsy by targeting the same signaling pathways.

## ONLINE METHODS

### The natural history of Dravet syndrome patients with the GABRG2(Q390X) mutation

The GABRG2(Q390X) mutation is associated with two small pedigrees of Dravet syndrome. One pedigree was reported by Harkin et al.,<sup>7</sup>. The other patient was identified by our U.K. collaborator Dr. Mark Rees.

The history of the patient in Harkin's report has been mentioned in two papers<sup>7,42</sup>. In Harkin's paper<sup>7</sup>, the patient's history was documented as "The patient had had a severe phenotype of GEFS+, which was initially regarded as MAE, but further history showed she had SMEI. She had multiple clonic seizures affecting the right upper limb, associated with fever at age 3 months. She had many such focal febrile seizures, as well as afebrile GTCS. But she did not have convulsive status epilepticus. Absence, myoclonic, and atonic seizures began at age 3–4 years. Myoclonus involving both upper limbs was prominent on examination and was exacerbated with lamotrigine. From age 17 years, she had continuous irregular myoclonus of her right upper limb; by age 22 years, she had 1–2 GTCS/year and 1–2 absence seizures. EEGs became more active over time and showed frequent paroxysms of irregular generalized polyspike-wave activity brought out by photic stimulation. MRI was normal. Early motor developmental milestones were normal, but speech was delayed. Neuropsychological assessment at age 14 years placed her in the moderately intellectually disabled range, without lateralizing features."

In Jansen's paper<sup>42</sup>, the patient was reported when she was 26 years old. Her age of seizure onset was 3 months. She first had febrile seizures, then she had TCS, myoclonic seizures (MS), absence seizures (AS), complex partial seizures (CPS) and tonic seizures (TS). Her diagnosis is SMEI. She had TCS, CPS and AS when she was at 26 years old. Motor signs were not present. In Jansen's paper, MRI scans were available in 10 patients. Unilateral hippocampal atrophy was noted in 2, generalized atrophy in 2 and 6 were normal. However, the authors did not specify which mutation had brain atrophy. To our knowledge, this is the only study that reports the natural history of Dravet syndrome with the GABRG2(Q390X) mutation.

The history of the patient identified by Dr. Mark Rees was unclear because the finding has not been published. However, per our communication with Dr. Rees, the child was very cognitively impaired and had refractory seizures but other information was not available.

### Mice

The *Gabrg2*<sup>+Q390X</sup> KI mouse was generated in collaboration with the Macdonald laboratory and Dr. Siu-Pok Yee at University Connecticut Health Center. Briefly, genomic DNA containing *Gabrg2* was retrieved from the BAC, RP23-233N1, which was generated

using DNA isolated from C57BL/6J mice. The targeting vector was prepared by recombineering as described<sup>43</sup>. The targeting vector containing the 5' long arm, which included exon 8, was approximately 5 kb followed by the LoxP-PGK-neo-LoxP cassette and exon 9 with the Q390X point mutation, which comprised the 3kb 3' short arm. A DraI restriction endonuclease site was engineered into the mutant *Gabrg2* allele to help distinguish the mutant from the wild-type allele. Targeted mice were bred with Hprt-Cre mice to remove the PGK-neo cassette to generate the mutant KI mouse. The targeting vector containing the 5' arm, which includes exon 8, is approximately 5 kb followed by the LoxP-PGK-neo-LoxP cassette and exon 9 with the Q390X (C1165T) point mutation, which comprise the 7kb 3' arm. The vector was linearized by NotI digestion prior to electroporation into ES cells, which was derived from F1 (C57BL/6J/129Svj) embryo. After electroporation into ES cells and G418 and Ganc selection, the targeted ES clones were identified by using long range PCR followed by PCR/sequencing to confirm the presence of the C1165T point mutation. Chimeric mice were generated by morula->ES cell aggregation and then bred with Hprt-Cre mice to remove the PGK-neo cassette and screened for germline transmission.

The primer pairs flanking the LoxP site for genotyping were gtF 5'-ATGGCGATGGAAGTTGACA and gtR: 5'-TGATGTTGCTCATGCCTCTC. The PCR fragment for the wild-type allele was 323 bp while the fragment for the mutant allele was 405 bp. The *Gabrg2*<sup>+/-</sup> KO mouse line was provided by Dr. Bernard Luscher (Penn State University)<sup>18</sup>. The mice used for biochemistry, immunohistochemistry and electrophysiology studies were from mixed C57BL/6J/129Svj background. The mice used for EEG recordings and neurobehavioral experiments were congenic lines and were bred into C57Bl/6J mice for at least 8 generations. All behavioral tests were done blind to mouse genotype with age matched littermates.

### Animal pairing and data acquisition for biochemistry study

All wild-type and mutant mice from the heterozygous *Gabrg2*<sup>+/*Q390X*</sup> KI and *Gabrg2*<sup>+/-</sup> KO lines used for biochemistry were gender matched littermates from each line. There was no sharing of wild-type mice between KI and KO lines. The wild-type and mutant mice were paired before the experiments. All the experiments were run in parallel. Each pair of wild-type and mutant KI or KO mice were sacrificed at the same time, the samples were prepared at the same time, samples from the four brain regions (cortex, cerebellum, hippocampus and thalamus) of each pair were run at the same time in the same gel. Each data point for wild-type and mutant mice were from the same membrane, and the protein of interest was normalized to the loading control Na<sup>+</sup>/K<sup>+</sup>-ATPase or GAPDH band from the same membrane each time.

### Plasmid and antibodies

The human  $\gamma 2$ (Q390X) and  $\gamma 2$ (Q390X)<sup>YFP</sup> subunit plasmids were described in a previous study<sup>10</sup>. Rabbit polyclonal anti- $\gamma 2$  subunit antibody (224-003, 1:300) was purchased from Synaptic System. Mouse monoclonal anti- $\gamma 2$  subunit antibody used in Figure 7d was a gift provided by Dr. Suchitra Joshi from Dr. Jeedep Kapur in Department of Neurology, University of Virginia, Health Sciences Center, Charlottesville, Virginia) (1:50). The

specificity of this antibody has been validated by Dr. Kapur's laboratory, and the antibody is commercially available<sup>44</sup>. Mouse monoclonal anti  $\alpha 1$ (N95/35) (1:1000) was from the University of California Davis/National Institutes of Health NeuroMab Facility. Rabbit anti-cleaved caspase 3 (9664S, 1:300) was from Cell Signaling Technology. The mouse monoclonal anti-neuronal nuclei (NeuN) antibody was from Millipore (MAB377, 1:100) or from Abcam (ab 104224, 1:100). The rabbit polyclonal anti-Er81 (AB10554, 1:100) and Trb1 (b81086) antibodies were from Millipore or Abcam. The mouse monoclonal GADD153 (AB11419, 1:100) antibody was purchased from Abcam. The rabbit anti-Calbindin D-28K antibody (CB38, 1:200) was from Swant. For protein loading internal controls, mouse monoclonal anti- $\text{Na}^+/\text{K}^+$ ATPase  $\alpha$  subunit (a6F, 1:1000) was from the Developmental Studies Hybridoma Bank, and the rabbit polyclonal GAPDH antibody (AB9485, 1:2000) was from Abcam. Mouse monoclonal  $\beta$ -Tubulin antibody (T8328, 1:500) was from Sigma. The fluorescently conjugated goat anti rabbit-680 (926-32221) and goat anti mouse-800 (926-32210) secondary antibodies were from LI-Cor (1:10,000).

### Brain slice immunohistochemistry

We used brain sections both with the conventional paraffin embedding method and with the short fixation protocol to preserve the postsynaptic proteins<sup>45</sup>. TUNEL staining was performed with the TACS 2 TdT-Fluor *in situ* apoptosis detection kit from Trevigen following the manufacturer's instructions and as performed in a previous study<sup>46, 47</sup>.

For freshly prepared brain tissues, mice were not perfused, and the brains were directly blocked and shortly fixed in 4% paraformaldehyde for 30 min and then maintained in 30% sucrose before sectioning on cryostat. The brains were sectioned at 15  $\mu\text{m}$ . The sectioned tissues were stored at  $-20^\circ$  before staining and discarded after 1 month. For paraffin embedded brain tissue preparations, mice were transcardially perfused with a fixative of 2% paraformaldehyde, 2% glutaraldehyde, and 0.2% picric acid in 0.1 M sodium phosphate, pH 7.2, and the brains were postfixed in 4% paraformaldehyde overnight at  $4^\circ\text{C}$ . The brains were preserved in 70% ethanol for 2 hrs and blocked and then processed by the Vanderbilt Pathology core with the standard procedure in the core. Paraffin embedded tissues were sectioned at 5  $\mu\text{m}$  using a microtome and stored at room temperature. The sectioned brain slices were mounted on Superfrost Plus slides for histochemical and immunohistochemical studies. The brain slices were routinely deparaffinized, rehydrated and antigen retrieved for 10 min at  $95^\circ\text{C}$ . The slices were then blocked for endogenous peroxidase activity with 3%  $\text{H}_2\text{O}_2$  solution for 10 min, permeabilized with 0.4% triton for 10 min and blocked with 0.2%/0.2% BSA/Triton for 1 hr followed by immunoreaction with specifically targeted antibodies overnight. The slices were then gently washed with 0.1% BSA/PBA three times before incubating with secondary antibodies. The slices were then processed with gradient alcohol (75%, 95% and 100%) and rinsed with the hydrophobic clearing agent xylene for 2 min twice and DAB reaction before being sealed with coverslips or directly sealed with ProLong Gold antifade mounting medium (Molecular Probes) for slices with fluorophore conjugated antibodies. The nuclei were either counterstained with hematoxylin for bright microscopy or with Topro-3 (1:500) for fluorescence microscopy.

### Immunohistochemistry related quantifications

For all  $\gamma 2$  subunit and caspase 3 protein intensity measurements, raw values of the protein intensity in the somatic region were measured in ImageJ. A total 10–12 randomly chosen non-overlapping fields from 3 consecutive sections per mouse were measured each time. All the neurons were included in each field. The mean value was taken as  $n = 1$  for each mouse. If the staining was with fluorophore-conjugated secondary antibodies, the nuclear region of the same cells was used as background because the boundary of the nuclei was relatively clear. If the staining was for light microscopy with DAB, the adjacent neuropil region was used as background because the boundary of the nuclei was not as clear. The protein intensity value of the somatic region for each cell was equal to the value of the somatic region subtracting the background value. In Figure 6C, the non-somatic fluorescence density value was the direct measurements of the neuropil region. The cell counting for caspase 3, calbindin D-28K and TUNEL positive cells as well as the NeuN positive cells co-labeled with cortical layers V or VI markers Er81 and Trb1 were quantified based on our previous study<sup>47</sup>. The mean positive staining was determined by counting 10–12 non-overlapping fields in specific layers in brain sections or in randomly chosen fields in cultures under 63X objective. The 10–12 non-overlapping fields were from 3 sections in each mouse or 3 dishes for each genotype in cultures for each experiment. The counts of 3 sections or 3 dishes were averaged and taken as  $n = 1$ . For the quantifications of the protein intensity in the somatic region in the immunohistochemistry, ImageJ was used.

### Digital histology and unbiased cell counting

For the brain sections with good representation of somatosensory cortex zone 1 and 2 (S1-2), we used the interaural 2.22 mm, Bregma 1.58 mm reference point based on the mouse brain atlas and cut 6–8 rostral sections at intervals of 5  $\mu\text{m}$  from each mouse brain for the assay in cortex, hippocampus and thalamus. We prepared the cerebellar sections separately. The mouse brains were cut sagittally across the midline and 6–8 consecutive sections at intervals of 5  $\mu\text{m}$  were prepared parasagittally starting from the midline in the right hemisphere. The images were acquired automatically by computer, and the image processing parameters were determined by the core personnel who were blind to mouse genotype. All the images were scanned at 20X and viewed with 7X. The total number of  $5 \times 10^5 \mu\text{m}^2$  in somatosensory cortex were quantified manually by a person blind to genotype or by MetaMorph software. The cell counts of the 6–8 consecutive sections were averaged and taken as one of 5 pairs of mice.

### Subcellular fractionation and isolation of synaptosomes

The procedures of subcellular fractionation were modified from a previous study<sup>48</sup>. Briefly, after quickly removing the brains, regions of interest were dissected and homogenized in pre-chilled homogenization HEPES buffered sucrose buffer (HBS containing 0.32 M sucrose, 10 mM HEPES, pH 7.4, 2mM EDTA) with a ratio of 10 ml buffer:1 g of brain tissue (each mouse brain is around 0.4g) with 10–15 strokes. The homogenates were then spun down at 1000 g for 10 min to remove the cell debris and nuclei. The pellet was taken as P1. The supernatant was taken as S1, and S1 was centrifuged at 13,800 g for 20 min. The S1 pellet was taken as P2, and the supernatant was taken as S2. S2 was the combination of

cytosol and light membranes, while P2 was crude synaptosomal fraction. P2 was resuspended with HBS buffer at 1:10 ratio and centrifuged at 13,800 g for 15 min (for wash). The washed pellet was then mixed with 9X vol ice cold H<sub>2</sub>O-protease inhibitors. After rapidly adjusting to 4 mM HEPES by using 1M HEPES (pH 7.4), the P2 suspension was then rotated for 30 min at 4°C, followed by spinning at 25,000 g for 20 min. The pellet was taken as P3 and resuspended by adding 1.5 ml HBS buffer followed by discontinuous gradient sucrose ultracentrifuge. An equal volume (2.2 ml) of sucrose with different concentrations (1.4 M, 1.2 M, 1.0 M to 0.8 M) was added from bottom to top in the tube. The sample (1.5 ml) of P3 was added to the top of the sucrose layers. The sucrose tube containing the sample of P3 was then centrifuged at 150,000 g for 1 hr, and then each layer of interest was carefully collected and stored at -80°C. The synaptosome layer (spm) was at 1.0/1.2 M sucrose interface.

### Live brain slice biotinylation

The protocol was based on a previous study<sup>20</sup>. Briefly, the brain slices were incubated for 45 min at 4°C in aCSF that contained 1 mg/ml of the membrane-impermeable, biotinylation reagent, sulfosuccinimidyl-2-(biotinamido)-ethyl-1,3'-dithiopropionate (Sulfo-NHS-SS-biotin; Thermo Scientific). After biotinylation, the slices were washed with 0.1 M glycine in aCSF. The cortices were dissected based on the region of interest and sonicated in radioimmunoprecipitation assay (RIPA) solution (20 mM Tris, pH 7.4, 1% Triton X-100, 250 mM NaCl) that also contained protease inhibitor mixture (1:100, Sigma-Aldrich), 0.5% deoxycholate and 0.1% SDS.

### Brain slice preparation and recording

Recordings of GABAergic mIPSCs were obtained from layer VI somatosensory cortex neurons in brain slices as previously described<sup>20</sup>. Coronal brain slice sections (300 µm) were made using a vibratome in ice-cooled solution containing (in mM) 214 sucrose, 2.5 KCl, 1.25 NaH<sub>2</sub>PO<sub>4</sub>, 0.5 CaCl<sub>2</sub>, 10 MgSO<sub>4</sub>, 24 NaHCO<sub>3</sub>, and 11 D-glucose, pH 7.4 bubbled with 95% O<sub>2</sub>/5% CO<sub>2</sub> at 4°C. Slices were then incubated in oxygenated artificial cerebrospinal fluid (ACSF) at 36°C for 30 min. After this, slices were kept at room temperature for at least 1 hr before recording on a Nikon Eclipse FN-1 IR-DIC microscope at room temperature. Pipette internal solution contained (in mM): 135 CsCl, 10 EGTA, 10 HEPES, 5 ATP-Mg, and QX-314 (5 mM) (pH 7.25, 290–295 mOsm), and recording micropipette resistances were 2 – 4 MΩ. Whole-cell patch clamp recordings were made at room temperature from layer VI pyramidal neurons in SI/II somatosensory cortex visualized with an upright Nikon eclipse FN-1 IR-DIC microscope. Neurons in the layer above the white matter with a typical apical dendrite and large soma (smaller than the layer V neuronal somata) were chosen for recordings. Data were collected using a MultiClamp 700B amplifier with compensation for series resistance (70%) and cell capacitance. Data were filtered at 2 kHz and digitized at 20 kHz using a Digidata 1440A AD converter.

### Synchronized EEG recordings and analysis

Synchronized video EEGs were recorded from 8 week to 4 month old C57BL/6J mice one week after electrode implantation and recorded with synchronized EEG monitoring system from Pinnacle Technology based on previous study<sup>49</sup>. Briefly, mice were anesthetized with

1–3% isoflurane and four epidural electrodes (stainless steel screws affixed to one head mount) were placed on the brain surface and secured in place with dental cement and surgical stitches. EMG leads were inserted into the trapezius muscle. Mice were allowed to recover from the EEG head mount implantation surgery for one week before EEG recording. Video-EEG monitoring lasted for 24–48 hrs, and mice were freely moving during EEG recordings. Mouse behaviors such as behavioral arrest, myoclonic jerks or generalized tonic clonic seizures during the EEG recordings were identified to determine if mice exhibit behavioral seizures. At least 24 hours of baseline EEG recordings were obtained and analyzed for each mouse.

### Open field test

Open field test was performed based on the standard protocol in Vanderbilt Neurobehavior core. Briefly, each individual mouse was placed into an open field activity chamber (Med Associates, 27 × 27 × 20.3 cm) that contained within light- and air-controlled environmental chambers for 60 min. Location and movement were detected by the interruption of infrared beams by the body of the mouse (16 photocells in each horizontal direction, as well as 16 photocells elevated 4cm to measure rearing) and were measured by the Med Associates Activity Monitoring program. Total distance traveled and time resting in center (50% of area) and peripheral zone were measured. The open field arena was cleaned with 70% ethanol and wiped with paper towels between each trial.

### Elevated zero maze test

The elevated zero maze is a modification of the elevated plus maze used for assessing anxiety-related behaviors. The elevated circular platform (40 cm off the ground, 50 cm in diameter) had two enclosed arenas opposite each other (5 cm wide with 15 cm high walls) and two open arenas (5 cm wide). Briefly, each mouse was lowered by its tail into the open arena of the maze and allowed to explore the maze for 300 s. The whole circular platform was cleaned with 70% ethanol and wiped with paper towels between each animal. Activity of the mouse was monitored via an overhead camera connected to a computer in a separate room using video acquisition and ANY-maze analysis software (Stoelting, Wood Dale, IL). Data analyzed included time spent in the open versus closed arms, the number of entry in the open arms.

### Protein structure prediction and docking

We used MUFOLD<sup>50</sup> to predict the protein structures. The docking was performed by symmetric docking of SymmDock between two  $\gamma$ 2 subunits and by general docking of PatchDock between the  $\gamma$ 2 and  $\alpha$ 1 subunits<sup>51</sup>. Chimera (UCSF Chimera--a visualization system for exploratory research and analysis<sup>52</sup>) was used to display the protein structures.

### Statistical analysis

IDVs were quantified by using the Quantity One or Odyssey fluorescence imaging system (Li-Cor). The fluorescence intensity values were quantified by using ImageJ. Data were expressed as mean ± S.E.M values and analyzed with Graphpad Prism 5.0 software. Statistical significance of immunoblot and cell imaging data was determined by two-way

ANOVA with Bonferroni posttests, a Student's unpaired t test or, if appropriate, single-value t test. For the comparison of GABAergic mIPSC electrophysiology data, a Kolmogorov-Smirnov test was used to determine the cumulative probabilities, the distribution of wild-type and the mutant mIPSC peak amplitudes. The behavioral data was analyzed by a distribution-free Mann-Whitney U test as well as Student's t test. No statistical methods were used to pre-determine sample sizes, but our sample sizes are similar to those reported in previous publications<sup>10, 19–20</sup>. Data distribution was assumed to be normal, but this was not formally tested. All analyses used an alpha level of 0.05 to determine statistical significance.

## Supplementary Material

Refer to Web version on PubMed Central for supplementary material.

## Acknowledgments

Research was supported by grants from Citizen United for Research in Epilepsy (CURE), Dravet syndrome foundation (DSF), Dravet.org which is previously named IDEAleague, Vanderbilt Clinical and Translation Science Award and NINDS R01 NS082635 to J.Q.K, NINDS R01 NS51590 to R.L.M and R01 GM100701 to D.X, NICHD Grant No. P30HD15052 to Vanderbilt Kennedy Center. Thanks to the Vanderbilt Translational Pathology core for the service in tissue preparation and immunostaining and Dr. Kelli Boyd for consultation on immunohistochemistry. Thanks to Keliene Marie Verdier and Dr. Aurea Pimenta for animal husbandry, Zhong Liu and Dr. John Allison for assistance in neurobehavioral tests and Shuai Zeng for computational assistance. Thanks to Dr. Suchitra Joshi in Dr. Jadeep Kapur's lab at University of Virginia School of Medicine for providing mouse monoclonal anti- $\gamma 2$  subunit antibody. Thanks to Dr. Lily Wang at Vanderbilt University, Department of Biostatistics for providing consultation on statistics and Dr. Ty Abel at Vanderbilt University, Department of Pathology for consultation on stereology and cell counting

## Reference List

1. Noebels JL. Exploring new gene discoveries in idiopathic generalized epilepsy. *Epilepsia*. 2003; 44(Suppl 2):16–21. [PubMed: 12752457]
2. Heron SE, et al. De novo SCN1A mutations in Dravet syndrome and related epileptic encephalopathies are largely of paternal origin. *J Med Genet*. 2010; 47:137–141. [PubMed: 19589774]
3. Shi X, et al. Missense mutation of the sodium channel gene SCN2A causes Dravet syndrome. *Brain Dev*. 2009; 31:758–762. [PubMed: 19783390]
4. Patino GA, et al. A functional null mutation of SCN1B in a patient with Dravet syndrome. *J Neurosci*. 2009; 29:10764–10778. [PubMed: 19710327]
5. Ogiwara I, et al. A homozygous mutation of voltage-gated sodium channel beta(I) gene SCN1B in a patient with Dravet syndrome. *Epilepsia*. 2012; 53:e200–e203. [PubMed: 23148524]
6. Ishii A, et al. Association of nonsense mutation in GABRG2 with abnormal trafficking of GABAA receptors in severe epilepsy. *Epilepsy Res*. 2014; 108:420–432. [PubMed: 24480790]
7. Harkin LA, et al. Truncation of the GABA(A)-receptor gamma2 subunit in a family with generalized epilepsy with febrile seizures plus. *Am J Hum Genet*. 2002; 70:530–536. [PubMed: 11748509]
8. Carvill GL, et al. GABRA1 and STXBP1: Novel genetic causes of Dravet syndrome. *Neurology*. 2014
9. Kang JQ, Shen W, Lee M, Gallagher MJ, Macdonald RL. Slow degradation and aggregation in vitro of mutant GABAA receptor gamma2(Q351X) subunits associated with epilepsy. *J Neurosci*. 2010; 30:13895–13905. [PubMed: 20943930]



10. Kang JQ, Shen W, Macdonald RL. The GABRG2 mutation, Q351X, associated with generalized epilepsy with febrile seizures plus, has both loss of function and dominant-negative suppression. *J Neurosci.* 2009; 29:2845–2856. [PubMed: 19261880]
11. Kang JQ, Shen W, Macdonald RL. Trafficking-deficient mutant GABRG2 subunit amount may modify epilepsy phenotype. *Ann Neurol.* 2013
12. Haynes CM, Titus EA, Cooper AA. Degradation of misfolded proteins prevents ER-derived oxidative stress and cell death. *Mol Cell.* 2004; 15:767–776. [PubMed: 15350220]
13. Crestani F, et al. Decreased GABAA-receptor clustering results in enhanced anxiety and a bias for threat cues. *Nat Neurosci.* 1999; 2:833–839. [PubMed: 10461223]
14. Reid CA, et al. Multiple molecular mechanisms for a single GABAA mutation in epilepsy. *Neurology.* 2013; 80:1003–1008. [PubMed: 23408872]
15. Hirsch LJ, et al. Abbreviated report of the NIH/NINDS workshop on sudden unexpected death in epilepsy. *Neurology.* 2011; 76:1932–1938. [PubMed: 21543734]
16. Kalume F, et al. Sudden unexpected death in a mouse model of Dravet syndrome. *J Clin Invest.* 2013; 123:1798–1808. [PubMed: 23524966]
17. Glasscock E, Yoo JW, Chen TT, Klassen TL, Noebels JL. Kv1.1 potassium channel deficiency reveals brain-driven cardiac dysfunction as a candidate mechanism for sudden unexplained death in epilepsy. *J Neurosci.* 2010; 30:5167–5175. [PubMed: 20392939]
18. Gunther U, et al. Benzodiazepine-insensitive mice generated by targeted disruption of the gamma 2 subunit gene of gamma-aminobutyric acid type A receptors. *Proc Natl Acad Sci U S A.* 1995; 92:7749–7753. [PubMed: 7644489]
19. Yu FH, et al. Reduced sodium current in GABAergic interneurons in a mouse model of severe myoclonic epilepsy in infancy. *Nat Neurosci.* 2006; 9:1142–1149. [PubMed: 16921370]
20. Zhou C, et al. Altered cortical GABAA receptor composition, physiology, and endocytosis in a mouse model of a human genetic absence epilepsy syndrome. *J Biol Chem.* 2013; 288:21458–21472. [PubMed: 23744069]
21. Donoghue JP, Ebner FF. The laminar distribution and ultrastructure of fibers projecting from three thalamic nuclei to the somatic sensory-motor cortex of the opossum. *J Comp Neurol.* 1981; 198:389–420. [PubMed: 7240451]
22. Alldred MJ, Mulder-Rosi J, Lingenfelter SE, Chen G, Luscher B. Distinct gamma2 subunit domains mediate clustering and synaptic function of postsynaptic GABAA receptors and gephyrin. *J Neurosci.* 2005; 25:594–603. [PubMed: 15659595]
23. Bucciantini M, et al. Inherent toxicity of aggregates implies a common mechanism for protein misfolding diseases. *Nature.* 2002; 416:507–511. [PubMed: 11932737]
24. Bence NF, Sampat RM, Kopito RR. Impairment of the ubiquitin-proteasome system by protein aggregation. *Science.* 2001; 292:1552–1555. [PubMed: 11375494]
25. Williams AJ, Paulson HL. Polyglutamine neurodegeneration: protein misfolding revisited. *Trends Neurosci.* 2008; 31:521–528. [PubMed: 18778858]
26. Berke SJ, Paulson HL. Protein aggregation and the ubiquitin proteasome pathway: gaining the UPPer hand on neurodegeneration. *Curr Opin Genet Dev.* 2003; 13:253–261. [PubMed: 12787787]
27. Yang DS, et al. Neuronal apoptosis and autophagy cross talk in aging PS/APP mice, a model of Alzheimer's disease. *Am J Pathol.* 2008; 173:665–681. [PubMed: 18688038]
28. Dillin A, Cohen E. Ageing and protein aggregation-mediated disorders: from invertebrates to mammals. *Philos Trans R Soc Lond B Biol Sci.* 2011; 366:94–98. [PubMed: 21115535]
29. Douglas PM, Dillin A. Protein homeostasis and aging in neurodegeneration. *J Cell Biol.* 2010; 190:719–729. [PubMed: 20819932]
30. Balch WE, Morimoto RI, Dillin A, Kelly JW. Adapting proteostasis for disease intervention. *Science.* 2008; 319:916–919. [PubMed: 18276881]
31. Ross CA, Poirier MA. Protein aggregation and neurodegenerative disease. *Nat Med.* 2004; 10(Suppl):S10–S17. [PubMed: 15272267]
32. D'Amelio M, Sheng M, Cecconi F. Caspase-3 in the central nervous system: beyond apoptosis. *Trends Neurosci.* 2012; 35:700–709. [PubMed: 22796265]

33. Li Z, et al. Caspase-3 activation via mitochondria is required for long-term depression and AMPA receptor internalization. *Cell*. 2010; 141:859–871. [PubMed: 20510932]
34. Berg AT, et al. Revised terminology and concepts for organization of seizures and epilepsies: report of the ILAE Commission on Classification and Terminology, 2005–2009. *Epilepsia*. 2010; 51:676–685. [PubMed: 20196795]
35. Betting LE, et al. MRI reveals structural abnormalities in patients with idiopathic generalized epilepsy. *Neurology*. 2006; 67:848–852. [PubMed: 16966549]
36. Perez A, et al. Brain morphometry of Dravet Syndrome. *Epilepsy Res*. 2014; 108:1326–1334. [PubMed: 25048308]
37. Ogiwara I, et al. Nav1.1 localizes to axons of parvalbumin-positive inhibitory interneurons: a circuit basis for epileptic seizures in mice carrying an *Scn1a* gene mutation. *J Neurosci*. 2007; 27:5903–5914. [PubMed: 17537961]
38. Ogiwara I, et al. Nav1.1 haploinsufficiency in excitatory neurons ameliorates seizure-associated sudden death in a mouse model of Dravet syndrome. *Hum Mol Genet*. 2013; 22:4784–4804. [PubMed: 23922229]
39. Laurie DJ, Wisden W, Seeburg PH. The distribution of thirteen GABAA receptor subunit mRNAs in the rat brain. III Embryonic and postnatal development. *J Neurosci*. 1992; 12:4151–4172. [PubMed: 1331359]
40. Kalume F, Yu FH, Westenbroek RE, Scheuer T, Catterall WA. Reduced sodium current in Purkinje neurons from Nav1.1 mutant mice: implications for ataxia in severe myoclonic epilepsy in infancy. *J Neurosci*. 2007; 27:11065–11074. [PubMed: 17928448]
41. Zeng LH, Rensing NR, Wong M. The mammalian target of rapamycin signaling pathway mediates epileptogenesis in a model of temporal lobe epilepsy. *J Neurosci*. 2009; 29:6964–6972. [PubMed: 19474323]
42. Jansen FE, et al. Severe myoclonic epilepsy of infancy (Dravet syndrome): recognition and diagnosis in adults. *Neurology*. 2006; 67:2224–2226. [PubMed: 17190949]
43. Lee MW, Chang AC, Sun DS, Hsu CY, Chang NC. Restricted expression of LUZP in neural lineage cells: a study in embryonic stem cells. *J Biomed Sci*. 2001; 8:504–511. [PubMed: 11702014]
44. Joshi S, Sun C, Kapur J. A mouse monoclonal antibody against the gamma2 subunit of GABAA receptors. *Hybridoma (Larchmt)*. 2011; 30:537–542. [PubMed: 22149279]
45. Notter T, Panzanelli P, Pfister S, Mircof D, Fritschy JM. A protocol for concurrent high-quality immunohistochemical and biochemical analyses in adult mouse central nervous system. *Eur J Neurosci*. 2014; 39:165–175. [PubMed: 24325300]
46. Chong ZZ, Kang JQ, Maiese K. Erythropoietin is a novel vascular protectant through activation of Akt1 and mitochondrial modulation of cysteine proteases. *Circulation*. 2002; 106:2973–2979. [PubMed: 12460881]
47. Kang JQ, Chong ZZ, Maiese K. Critical role for Akt1 in the modulation of apoptotic phosphatidylserine exposure and microglial activation. *Mol Pharmacol*. 2003; 64:557–569. [PubMed: 12920191]
48. Mao LM, et al. Stability of surface NMDA receptors controls synaptic and behavioral adaptations to amphetamine. *Nat Neurosci*. 2009; 12:602–610. [PubMed: 19349975]
49. Arain FM, Boyd KL, Gallagher MJ. Decreased viability and absence-like epilepsy in mice lacking or deficient in the GABAA receptor alpha1 subunit. *Epilepsia*. 2012; 53:e161–e165. [PubMed: 22812724]
50. Zhang J, et al. MUFOLD: A new solution for protein 3D structure prediction. *Proteins*. 2010; 78:1137–1152. [PubMed: 19927325]
51. Schneidman-Duhovny D, Inbar Y, Nussinov R, Wolfson HJ. Geometry-based flexible and symmetric protein docking. *Proteins*. 2005; 60:224–231. [PubMed: 15981269]
52. Pettersen EF, et al. UCSF Chimera--a visualization system for exploratory research and analysis. *J Comput Chem*. 2004; 25:1605–1612. [PubMed: 15264254]

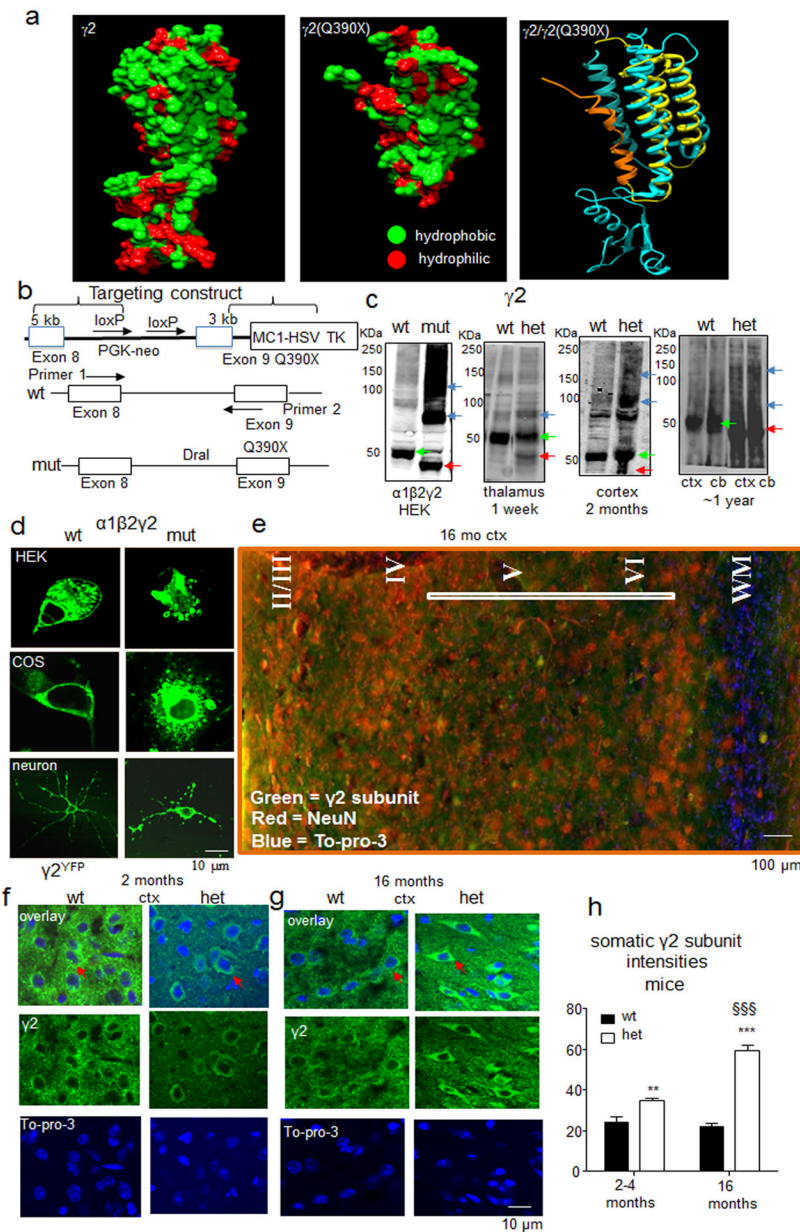


**Figure 1. The GABRG2(Q390X) mutation associated with the epileptic encephalopathy Dravet syndrome caused the mutant subunit to be aggregate prone and to accumulate intracellularly**  
**a**, Predicted structural models. The left and middle panels show protein surfaces of wild-type  $\gamma 2$  and mutant  $\gamma 2(Q390X)$  subunits, respectively, where green indicates hydrophobic residues and red shows hydrophilic (polar or charged) residues. The right panel shows the mutant and wild-type subunits superimposed with the same orientation as the left and middle panels ( $\gamma 2$  subunit in cyan/blue and  $\gamma 2(Q390X)$  subunit in yellow/orange). The transmembrane 4 (TM4)  $\alpha$ -helix (YARIFFPTAFCLFNLVYWVSYLYL) in the wild-type  $\gamma 2$  subunit and a new  $\alpha$ -helix (KDKDKKKKNPAPTIDIRPRSATI) in the mutant  $\gamma 2(Q390X)$  subunit are shown in highlight with edged representations. **b**, The *Gabrg2*<sup>+/<sup>Q390X</sup></sup> KI mouse was constructed with insertion of a DraI restriction site in the

mutant allele. **c**, Wild-type  $\gamma 2$  subunits or mutant  $\gamma 2(Q390X)$  subunit monomers and oligomers were detected in lysates from HEK 293T cells coexpressing  $\alpha 1\beta 2\gamma 2$  or  $\alpha 1\beta 2\gamma 2(Q390X)$  subunits (HEK), lysates from wild-type and KI mouse thalami (1 week), wild-type and *Gabrg2<sup>+ / Q390X</sup>* mouse cortical membrane preparations (2 months) and immunopurified  $\gamma 2$  subunits from wild-type and KI mouse cortex (cxt) and cerebellum (cb) (~1 year). **d**,  $\gamma 2(Q390X)$ , but not  $\gamma 2$ , subunits accumulated intracellularly in live  $\alpha 1\beta 2\gamma 2^{YFP}$  (wt) or  $\alpha 1\beta 2\gamma 2(Q390X)^{YFP}$  (mut) subunit-transfected HEK 293T cells (HEK) and COS-7 (COS) cells and  $\gamma 2^{YFP}$  or  $\gamma 2^{YFP}$  and  $\gamma 2(Q390X)^{YFP}$  subunit-transfected cultured rat cortical neurons. **e**. Image showing a coronal brain section of somatosensory cortex layers II–VI from a 16 month old wild-type mouse stained with anti- $\gamma 2$  subunit (green) and anti-NeuN (red) antibodies and with To-pro-3 (blue). White line designates the approximate layers surveyed in g and h. **f, g**, Freshly prepared brain sections from 2–4 months old (f) or over 16 months old (g) wild-type and KI littermates were immunostained with anti- $\gamma 2$  subunit antibody and visualized with Alexa-488 fluorophores (green) under confocal microscopy. The nuclei were stained with To-pro-3 (blue). **h**, Fluorescence intensities of  $\gamma 2$  subunits conjugated with Alexa-488 fluorophores in cortical brain sections from wild-type and heterozygous mice were quantified. (unpaired t test,  $p = 0.008$  wt vs het for 2–4 months old,  $p < 0.0001$  wt vs het for 16 months and 2–4 months vs 16 months ( $n = 5$  for 5 pairs of mice; 5 independent experiments, error bars are s.e.m.) (\*\*  $p < 0.01$ ; \*\*\* $p < 0.001$  vs wt, §§§ $p < 0.001$  vs 2–4 months old mice. In c, the red arrows designate the mutant  $\gamma 2$  subunit monomers, the green arrows designate the wild-type  $\gamma 2$  subunits and the blue arrows designate the mutant  $\gamma 2$  subunit aggregates. In f and g, the red arrows designate the somatic regions of individual cells.

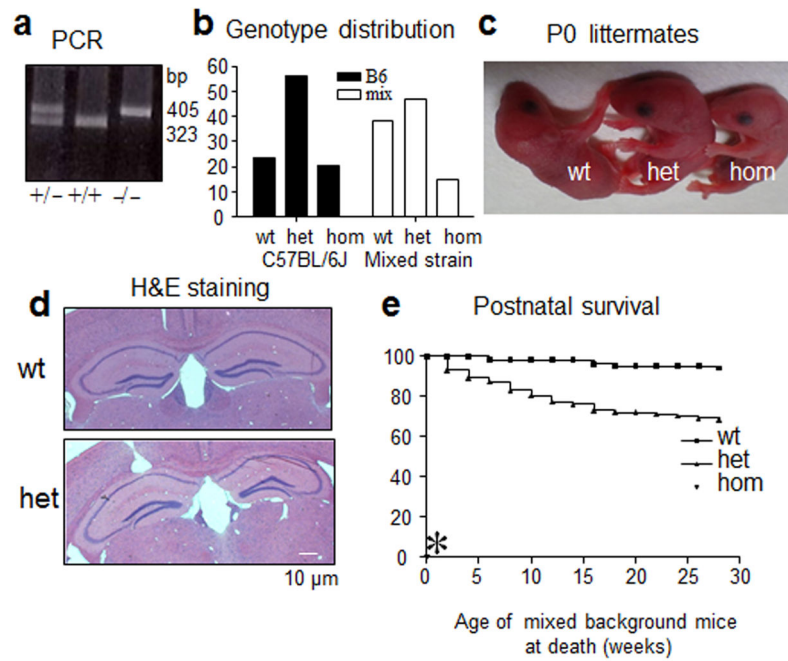


**Figure 2. *Gabrg2*<sup>+/-Q390X</sup> KI mice had increased mortality both pre- and postnatally**  
**a**, The wild-type  $\gamma 2$  subunit allele PCR product was 323 bp while the mutant  $\gamma 2$  subunit allele product was 405 bp due to the insertion of an 82 bp fragment as shown in the PCR image for genotyping. **b**, The distribution of each genotype for pups in mixed C57Bl/6J/129Svj (n = 7 litters, 58 pups) and C57Bl/6J (n = 8 litters, 69 pups) backgrounds was plotted. **c**, Mutant P0 pups were grossly normal. **d**, Sections of cerebral cortex including the hippocampal formation were stained with hematoxylin and eosin. **e**, A survival plot was obtained that showed the percentage of surviving mice with each genotype for 30 postnatal weeks (n = 51 for wt and 47 for het). Note that homozygous KI mice did not survive beyond P0 (asterisk).

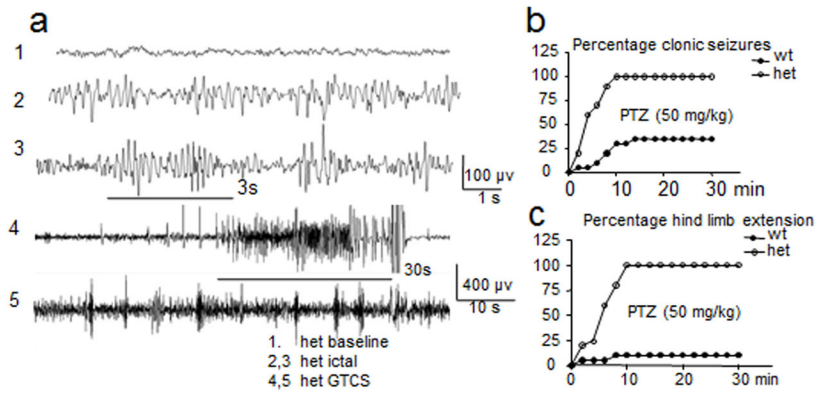


**Figure 3. *Gabrg2*<sup>+Q390X</sup> KI mice had severe seizures and behavioral comorbidities**  
**a**, Representative EEG recordings show that the heterozygous (het) KI mice had interictal periods without (het baseline) or with (het ictal) epileptiform activity and had spontaneous generalized tonic clonic seizures with epileptiform discharges (het GTCS). **b**, **c**, KI mice had lowered seizure threshold with intraperitoneal pentylenetetrazol (PTZ) administration (50 mg/kg). After PTZ injection, KI mice in the C57BL/6J background (open circles) progressed more rapidly to (b) clonic seizures and hind limb extension (c) than wild-type (wt) mice (filled circles) ( $n = 20$  mice for wt and 23 for het).

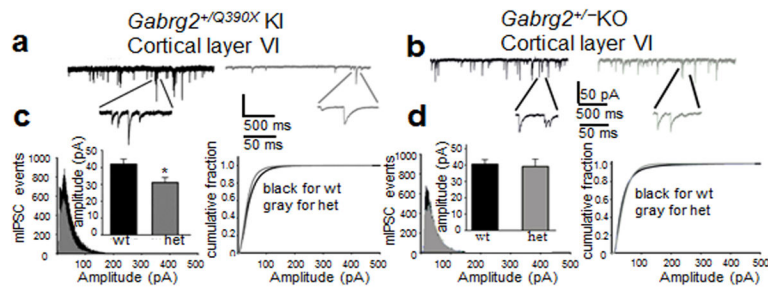


**Figure 4. The GABAergic mIPSCs from  $Gabrg2^{+/-Q390X}$  KI mice were not equivalent to those from  $Gabrg2^{+/-KO}$  mice**

**a, b**, Representative traces of GABAergic mIPSCs from cortical layer VI pyramidal neurons from two month old wild-type (wt) and heterozygous (het) KI (a) or KO (b) mice. **c, d**, mIPSC amplitudes were plotted as a function of frequency of occurrence and amplitude (inserts) and in cumulative histograms for both het KI (c) and KO (d) mice. (For KI mice,  $n = 15$  cells from 11 slices from 10 mice for wt and 11 cells from 8 slices from 8 mice for het, unpaired t test,  $p = 0.022$  wt vs het; For KO mice,  $n = 8$  cells from 6 slices from 5 mice for wt,  $n = 9$  cells from 7 slices from 6 het mice,  $p = 0.966$  wt vs het). Error bars are mean  $\pm$  s.e.m., \*  $p < 0.01$  vs wt).

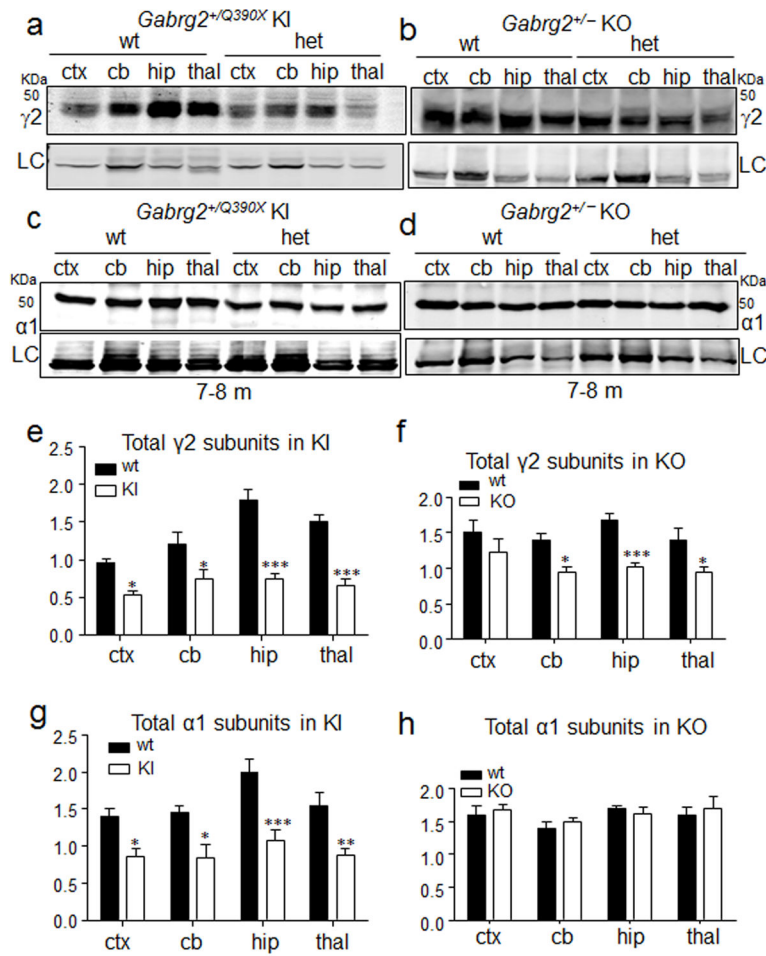


**Figure 5. *Gabrg2*<sup>+/-Q390X</sup> KI mice were not equivalent to *Gabrg2*<sup>+/-</sup> KO mice with respect to the remaining wild-type GABA<sub>A</sub> receptor subunit expression**

**a–d**, Lysates from different brain regions (cortex (ctx), cerebellum (cb), hippocampus (hip) and thal (thalamus)) from heterozygous (het) KO and KI mice were subjected to SDS-PAGE and immunoblotted with anti- $\gamma 2$  subunit antibody (a, b) or anti- $\alpha 1$  subunit antibody (c, d). **e–h**, Integrated density values (IDVs) for total  $\gamma 2$  and  $\alpha 1$  subunits from wild-type and het KI (e, g) or wild-type and het KO (f, h) mice were normalized to the Na<sup>+</sup>/K<sup>+</sup> ATPase or anti-glyceraldehyde-3-phosphate dehydrogenase (GAPDH) loading control (LC) in each specific brain region and plotted. (In e–h, \**p* < 0.05; \*\**p* < 0.01; \*\*\**p* < 0.001 vs wt. *n* = 5 pairs of mice for KI and 5 pairs of mice for KO, error bars are s.e.m. Full-length gels are presented in Supplementary Fig. 4. See Supplementary Methods checklist for full details of statistical tests.)



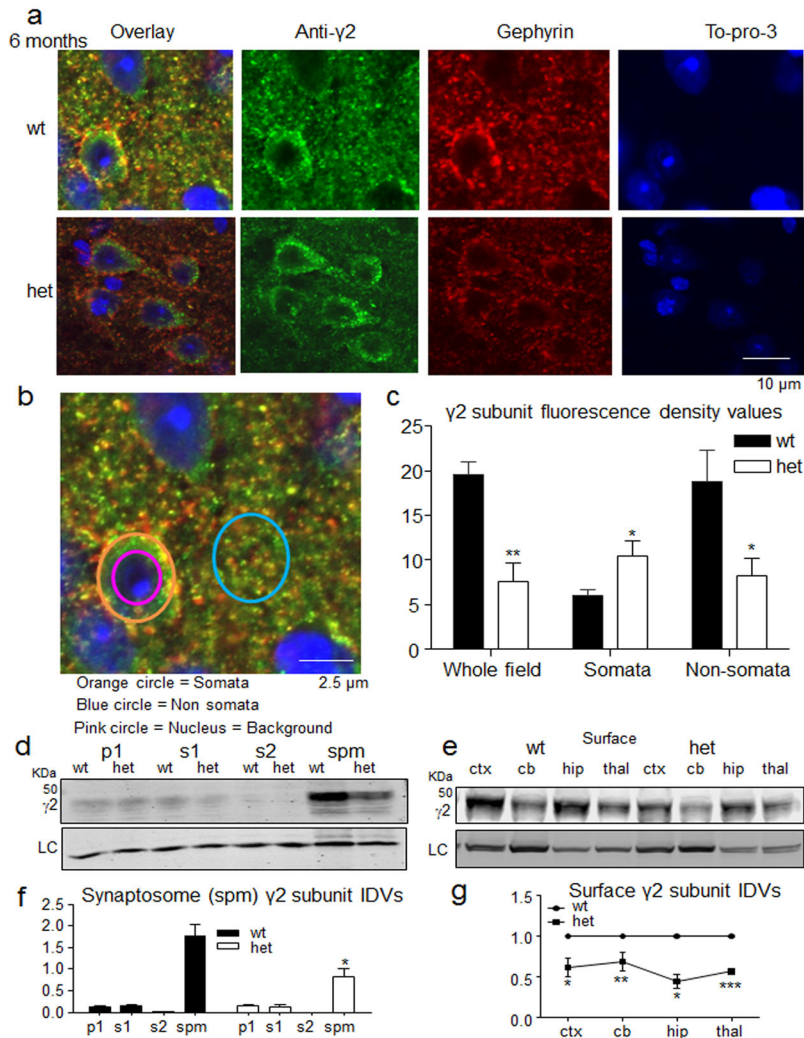


**Figure 6. Younger *Gabrg2*<sup>+/<sup>Q390X</sup> KI mice had increased  $\gamma$ 2 subunit accumulation in neuronal somata, but reduced expression of  $\gamma$ 2 subunits in synaptosomes and on the cell surface</sup>**

**a**, The brains from 6 month old wild-type and heterozygous (het) KI littermates were blocked, short fixed with 4% paraformaldehyde for 30 min and immersed in 30% sucrose overnight. The brain tissues were sectioned by cryostat at 15  $\mu$ m and stained with rabbit anti- $\gamma$ 2 subunit antibody (green), mouse anti-gephyrin antibody (red) and cellular nucleus marker To-pro-3 (blue). The presented images were from cortex layers V–VI. **b**, An enlarged image from the wt overlay was used to illustrate the quantification of the fluorescent intensity values in somatic and non-somatic regions with ImageJ. The fluorescent intensities of the whole field, somatic or non-somatic regions were measured. **c**, The fluorescence intensity values in the nuclei were used as background values that were subtracted in each condition. The total fluorescence intensity values from the whole field and non-somatic regions were reduced but were increased in the somata in the het mouse brains. ( $p = 0.0048$  for whole field,  $p = 0.0031$  for somata,  $p = 0.0136$  for nonsomata,  $n = 11$  mice for wt and 12 mice for het, unpaired t test). **d, f**, The forebrains of 2–4 months old mice were subfractionated. Equal amounts of protein from nuclei and cell debris (p1), total cytosol (s1), cytosol and light membrane (s2) and synaptosomes (spm) were analyzed by

SDS-PAGE and immunoblotted with anti- $\gamma 2$  subunit antibody. The protein IDVs in each fraction were normalized to their own loading control (LC)  $\text{Na}^+/\text{K}^+$  ATPase or  $\beta$ -Tubulin ( $p = 0.034$  wt vs het spm,  $n = 4$  pairs of mice, 4 independent experiments, unpaired t test). **e, g**, The surface proteins from the live mouse brain slices were biotinylated and analyzed by SDS-PAGE and immunoblotted with anti- $\gamma 2$  subunit antibody ( $p = 0.011$  for cor,  $p = 0.0088$  for cb,  $p = 0.0154$  for hip,  $p = 0.0007$  for thal,  $n = 4$  pairs of mice. One sample t test). (In c, f–g, \* $p < 0.05$ ; \*\* $p < 0.01$ , \*\*\* vs wt. Error bars are s.e.m., See Supplementary Methods Checklist for full details of statistical tests. Full-length gels for d and e are presented in Supplementary Fig. 4.)

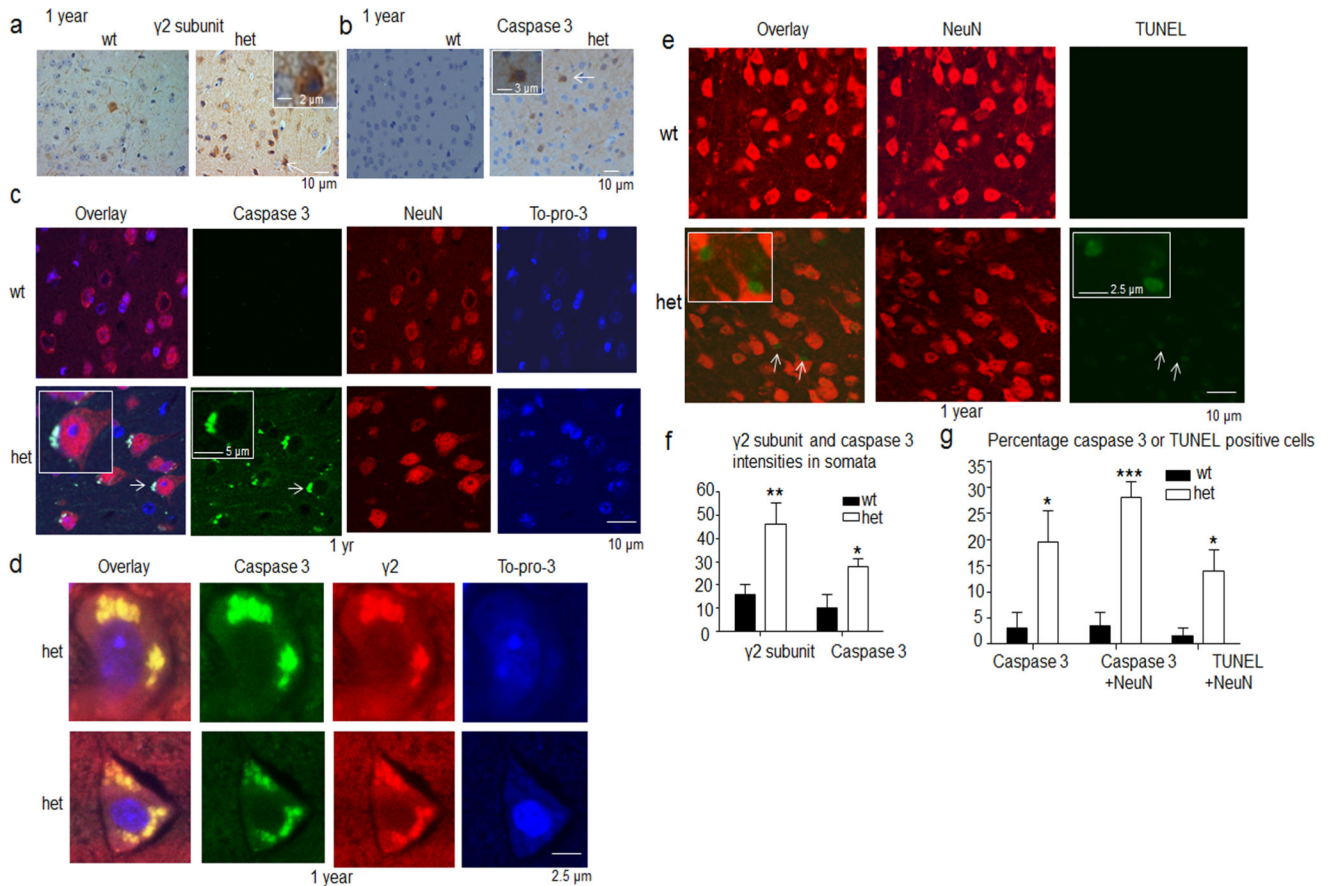


**Figure 7. Older *Gabrg2*<sup>+/Q390X</sup> KI mice had caspase 3 activation and neuronal death in the deep layers of cerebral cortex**

**a, b,** Brain sections from 1 year old wild-type (wt) and heterozygous (het) KI mice were stained with (a) rabbit anti- $\gamma 2$  subunit antibody or (b) rabbit cleaved caspase 3. **c–e,** Similar sections were stained for cleaved caspase 3 (green) in combination with (c) mouse monoclonal neuronal marker NeuN (red) and cellular nuclei marker To-pro-3 (blue), (d) mouse anti- $\gamma 2$  subunit (red) and cellular nuclei marker To-pro-3 (blue), or (e) NeuN (red) and cell death marker TUNEL (green). **f,** The  $\gamma 2$  subunit and cleaved caspase 3 protein density values in the cell somata were quantified using image J ( $p = 0.005$  for  $\gamma 2$  subunit,  $p = 0.0161$  for caspase 3 intensity,  $n = 12$  sections from 7 mice for wt and  $n = 11$  sections from 7 mice for het., unpaired t test). (\* $p < 0.05$ ; \*\* $p < 0.01$  vs wt,  $n = 12$  for wt and 11 for het). **g,** The cleaved caspase 3 positive staining cells in the total cellular population, the cleaved caspase 3 positive staining in NeuN positive cells and the TUNEL positive cells in the NeuN expressing populations were quantified and plotted ( $p = 0.0301$  for caspase 3,  $p < 0.0001$  for caspase 3 + NeuN,  $P < 0.0001$  for TUNEL.  $n = 7$  pairs of mice, unpaired t test. (In f–g, \* $p < 0.05$ ; \*\* $p < 0.01$  vs wt, \*\*\* $p < 0.001$  vs wt Error bars are s.e.m. See Supplementary Methods Checklist for full details of statistical tests.).

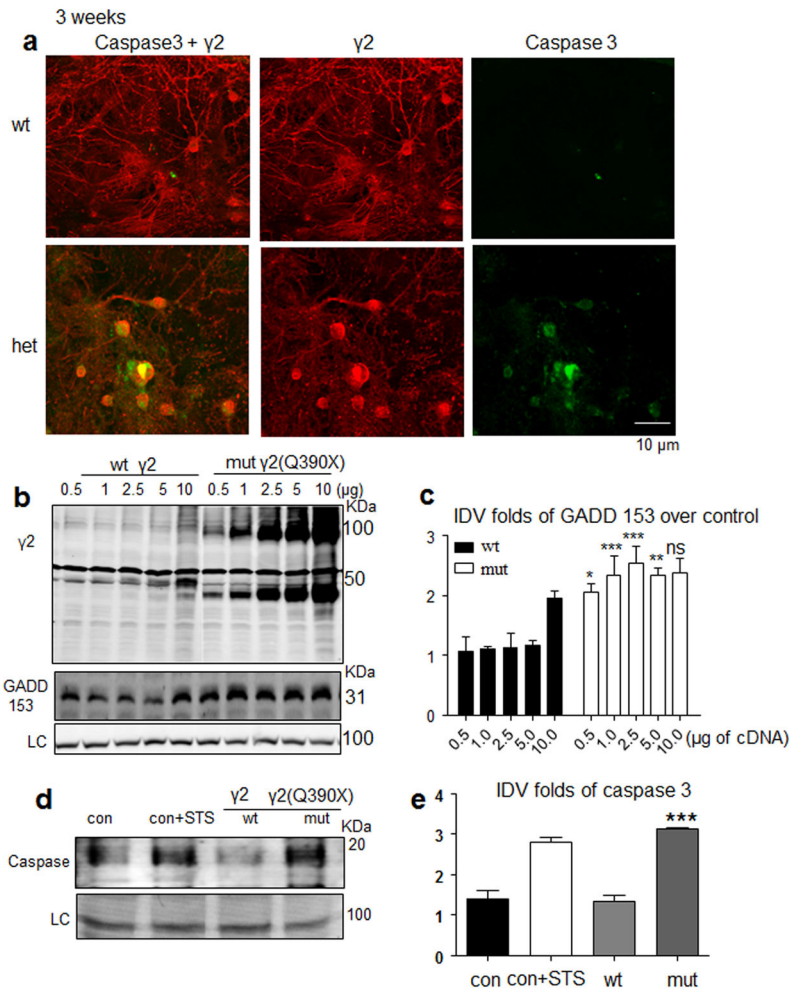


**Figure 8. Increased ER stress and caspase 3 activation were detected in cells expressing mutant  $\gamma 2(Q390X)$  subunits**

**a**, Hippocampal neurons from P0 wild-type and heterozygous (het) KI mice were grown in cell culture for three weeks, and neurons were stained with rabbit polyclonal anti-cleaved caspase 3 (green) and mouse monoclonal anti- $\gamma 2$  subunit (red) antibodies (**a**). **c**, **d**, Lysates from HEK 293T cells expressing  $\gamma 2$  or  $\gamma 2(Q390X)$  subunits with progressively increased cDNA concentrations were immunoblotted with either anti- $\gamma 2$  subunit or the ER stress hallmark anti-GADD153 antibody with an  $\text{Na}^+/\text{K}^+$  ATPase loading control (LC) (**c**), and the normalized GADD153 IDVs were plotted (\* $p < 0.05$ ; \*\* $p < 0.01$ , \*\*\* $p < 0.001$  vs wt of the same cDNA amount,  $n = 4$  different transfections. See Supplementary Methods Checklist for full details of statistical tests.) (**d**). **e**, **f**, HEK 293T cells were either untransfected (con) or transfected with  $\gamma 2$  (wt) or  $\gamma 2(Q390X)$  (mut) subunits. The apoptosis inducer staurosporine (3  $\mu\text{M}$ ) was applied for 4 hrs as positive control (con + STS). The cells were harvested 2 days after transfection and analyzed by SDS-PAGE and immunoblotted by the anti-cleaved caspase 3 (**e**). The IDVs for each condition were normalized to the loading control  $\text{Na}^+/\text{K}^+$  ATPase or  $\beta$ -tubulin and plotted (\*\*\* $p < 0.001$  vs wt,  $n = 4$  different

transfections (f). (Error bars are s.e.m.. See Supplementary Methods Checklist for full details of statistical tests. Full-length gel for e is presented in Supplementary Fig. 4.)

Author Manuscript

Author Manuscript

Author Manuscript

Author Manuscript